Frequency up-conversion imaging with 60-dB gain using picosecond optical parametric amplifier

Xiaoqing Li (李小青)[1,2], Jing Yang (杨 晶)[1*], Xinzhi Sheng (盛新志)[2], Jingyuan Zhang (张景园)[3], Dafu Cui (崔大复)[1], Qinjun Peng (彭钦军)[1], and Zuyan Xu (许祖彦)[1]

[1]*RCLPT, Key Lab of Functional Crystal and Laser Technology, Technical Institute of Physics and Chemistry, Chinese Academy of Sciences, Beijing 100190, China*

[2]*School of Science, Beijing Jiaotong University, Beijing 100044, China*

[3]*Department of Physics, Georgia Southern University, Statesboro, GA 30460, USA*

[*]*Corresponding author: yangjingeagle@163.com*

Received September 3, 2013; accepted September 25, 2013; posted online November 6, 2013

A weak infrared (IR) image amplifier with more than 60-dB optical gain and frequency up-conversion is developed from a picosecond (PS) 355-nm pumped gated optical parametric amplifier (OPA) in a β-BaB_2O_4 (BBO) crystal. The IR image at 1064 nm is amplified and up-converted into the visible region at 532 nm by parametric amplification and up-conversion. With the optimized optical gain, the lowest detectable energy of the image can be as low as 1.8 femto-Joule per pulse, which is three orders of magnitude lower than the detection limit of a charge-coupled device (CCD) camera. The transversal resolution of the OPA imaging is investigated, and the approaches for higher detection sensitivity and higher transversal resolution are proposed.

OCIS codes: 190.4970, 190.7220, 100.2980.
doi: 10.3788/COL201311.111901.

Frequency up-conversion imaging with high optical gain is beneficial in several applications such as chemistry, biomedical diagnosis, and remote sensing. In addition to the commonly used electronic devices, such as intensified and electron-multiplying charge-coupled devices (CCDs), nonlinear optics provides an efficient approach in the direct optical amplification for diverse mechanisms. These mechanisms include photorefractive effect[1], stimulated Raman scattering[2], stimulated Brillouin scattering[3], optical parametric amplification (OPA)[4], and etc. Compared with other candidates, the OPA-based imaging has the potential to simultaneously achieve frequency up-conversion, high optical gain, and polychromatic amplification. OPA has been performed as early as 1968[4], but its potential was not fully investigated until the progresses in picosecond (ps)/femtosecond (fs) laser systems and nonlinear crystals (NLCs) were realized[5–8]. In the fs region, Watson *et al.*[5] demonstrated a 40-dB gain with a fs OPA. Vaughan *et al.*[6] achieved 20-dB magnitude image amplification to the complex target with frequency up-conversion using fs OPA. In the ps region, more than 40-dB image amplification is also demonstrated without the frequency up-conversion[8]. Compared with the fs scheme, high gain is more difficult to obtain using the ps OPA. Therefore, studies on OPA-based high gain image amplifiers with frequency up-conversion still mainly focus in the fs region, with a maximum gain of no more than 40 dB.

In this letter, a high-gain infrared (IR) image amplifier based on an ultraviolet (UV)-pumped ps-OPA is demonstrated. The weak IR image is also up-converted into the visible region through parametric signal-to-idler up-conversion, and the optical gain is as high as 60 dB. After the amplification, the weak IR image can be detected using a CCD camera, which is more sensitive in the visible region. The limit of the detectable signal is three orders of magnitude more sensitive than the direct CCD camera imaging. This optical gain is two orders of magnitude higher than previously reported values.

OPA is a typical three-wave coupling process in an NLC. Under the phase-match condition, one photon of the pump beam at frequency ω_p is converted into a pair of photons with frequency of signal ω_s and idler ω_i under the restriction of energy conservation shown as

$$\hbar\omega_\mathrm{p} = \hbar\omega_\mathrm{s} + \hbar\omega_\mathrm{i}. \tag{1}$$

When a UV laser is adopted as a pump beam and a near-IR signal is injected into the OPA, the near-IR signal can be amplified, and the frequency up-converted and detected with a visible detector. The wavelength of the near-IR image can be extended to mid-IR as long as the NLC permits. The small signal gain coefficient g_0 of the IR signal beam is given by[9]

$$g_0 = \left[\left(\frac{\mu_0}{\varepsilon_0}\right)\frac{\omega_\mathrm{s}\omega_\mathrm{i}}{n_\mathrm{s}n_\mathrm{i}}\right]^{1/2} d_\mathrm{eff}A_\mathrm{p}, \tag{2}$$

where n_s and n_i represent the refractive indices for the signal and the idler waves, respectively, d_eff is the effective nonlinear coefficient, depending on the type of NLC and phase match, and A_p is the electric field of the pump beam, which is proportional to the square root of the power density I_p. To guarantee a net gain, $g_0 > \Delta k/2$ should be satisfied. In this letter, Δk is the phase mismatch. For the frequency up-conversion application, the energy gain (G) of the idler to the input signal is shown as

$$G = \frac{\omega_\mathrm{i}}{\omega_\mathrm{s}}\left[\frac{g_0}{g'}\sinh(g'L_\mathrm{c})\right]^2, \tag{3}$$

where $g' = \sqrt{g_0^2 - (\frac{\Delta k}{2})^2}$, and L_c is the length of the optical

 © 2013 Chinese Optics Letters

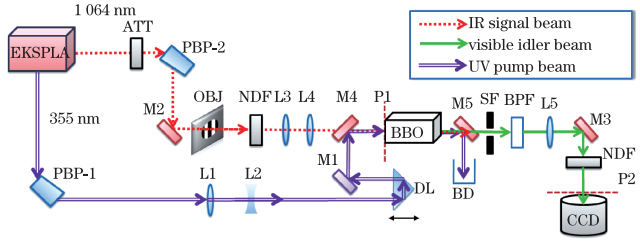

Fig. 1. Experimental setup. ATT: attenuator; PBP: Pellin-Broca prism; OBJ: object; NDF: neutral density filter; BPF: band pass filter; SF: spatial filter; DL: optical delay line. L1, L2, and L5: image lens; L3 and L4: telescope lens; M1-M3: highly reflective mirrors at 1064, 355, and 532 nm, respectively; M4-M5: dichroic mirror; BD: beam dump.

NLC. When the phase match is completely satisfied ($\Delta k = 0, g_0 = g'$), the gain factor of the OPA is simplified in

$$G = 2\left[\sinh(\alpha.d_{\text{eff}}.\sqrt{I_{\text{p}}}.L_{\text{c}})\right]^2, \tag{4}$$

where $\alpha = \frac{1}{\varepsilon_0}[\frac{2\mu_0\omega_{\text{s}}\omega_{\text{i}}}{n_{\text{s}}n_{\text{i}}n_{\text{p}}c}]^{1/2}$. The extra bonus of the frequency up-conversion is that the energy gain will multiply a factor of $\omega_{\text{i}}/\omega_{\text{s}}$, which is 2 in our experiment because the frequency of the idler is twice that of the signal. The factor can even be more if the image is in the mid-IR. A longer NLC and a higher pump intensity are evidently necessary to obtain a higher gain. However, a trade-off exists between the optical gain and the spatial resolution. According to the theory of amplification transfer function[10], phase mismatch Δk is deliberately introduced to obtain a higher resolution[11].

The experimental setup is shown in Fig. 1. An attenuated image pattern generated by the fundamental output of a 10-Hz, 1064-nm Nd:YAG laser (p-polarized, 30 ps, 2143-C, EKSPLA) is treated as the signal in the OPA. The third harmonics output of the same laser at 355 nm (p-polarized) is served as the pump beam. Thus, the idler beam is at 532 nm according to Eq. (1). A β-BaB_2O_4 (BBO) crystal is selected as the NLC because of its large nonlinear coefficient and acceptable damage threshold. BBO is cut at θ=29°and ϕ=0° for type-I phase-match ($o + o \rightarrow e$), and the corresponding effective nonlinear coefficient is 2 pm/V. The dimensions of the crystal are $5 \times 8 \times 10$ (mm) (W×H×L).

To remove other frequency components that may affect the OPA gain measurement, a Pellin–Broca Prism (PBP-1) is inserted into the beam path of a 355-nm pump laser. Then, its beam size is reduced to roughly 3.6 mm by a telescope consisting of two lenses (L_1 and L_2). The collinear OPA configuration is used so that the pump and the signal spatially overlap with each other. The temporal overlap between the signal and the pump beam is achieved by optical delay line. When the these requirements are all satisfied, the weak IR image can be amplified and up-converted into the visible region simultaneously. Dichroic mirrors M_4 (AR at 1064 nm and HR at 355 nm) and M_5 (AR at 532 nm and HR at 355 nm) are used to combine the signal with the pump beam and separate the idler output from the signal and pump beam, respectively. The residual pump beam is collected by a beam dump. To reduce the parametric fluorescence background with the increasing pump intensity, a spatial filter (SF) and a narrow band-pass filter (BPF) at 532 nm are used.

The signal beam at 1064 nm passes through the attenuator (ATT), which is a combination of a half-wave plate and a thin film polarizer, so that the energy of the signal laser can be continuously adjusted. A Pellin–Broca Prism (PBP-2) is also inserted into the beam path to eliminate irrelevant frequencies. Then, the signal beam illuminates a two-dimensional (2D) object (OBJ), which is a glass plate coated with standard resolution patterns; the uncoated parts transmit the signal beam. A set of calibrated neutral density filters (NDFs) is inserted to further reduce the signal. A cascaded imaging system is used, with the image lens L_3 (focal length: fl = 400 mm) and L_4 (fl = 300 mm). The target is imaged at plane P1, which is also the input facet of the BBO crystal, where the weak image is amplified. Finally, the amplified image is relay imaged by L5 at P2, where it is recorded by a CCD camera or an energy meter. The size of the signal beam is reduced to one-fourth of its original size by controlling the magnification of the imaging system composed of L3 and L4. The distances from the target to L3, from L3 to L4, and from L4 to the nonlinear optical crystal are set to 880, 50, and 209 mm, respectively.

The optical gain of the IR signal versus the pump intensity is investigated first. The energies of the signal and output idler beams are both measured with a sensitive energy meter (NOVA-II, Ophir, Israel) and an nJ-energy detector (PD10, Ophir, Israel). The image is recorded by a 12-bit CCD camera (SCOR-20, Spiricon, USA), which is located at the position of the BBO crystal in Fig. 1. The lowest energy detectable by our CCD camera is calibrated. The 1064-nm signal is continuously attenuated using the ATT and NDFs. The image becomes under-detectable with the CCD when the energy of the signal is reduced to 1.9 pJ per pulse. The signal is further reduced to around 1 pJ per pulse. Then, the pump beam is introduced, and the amplified and frequency up-converted image is observed. NDFs are used in front of the idler beam to avoid saturation of the CCD camera.

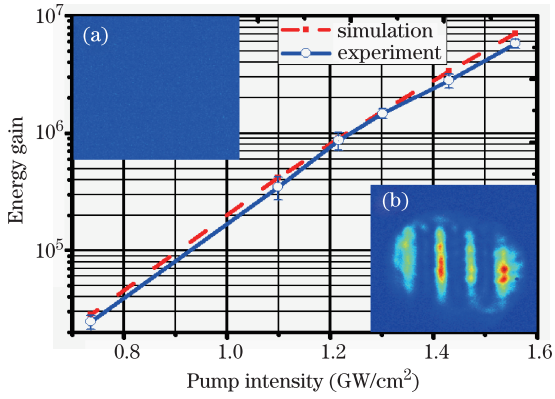

Fig. 2. (Color online) Energy gain versus pump intensity. Red dashed curve is the numerical simulation from the three-wave coupling, and the blue solid curve is the experimental energy gain versus pump intensity. Inset (a) is under-detectable image without a pump beam, whereas inset (b) is the amplified image under 1.56 GW/cm^2 pump intensity.

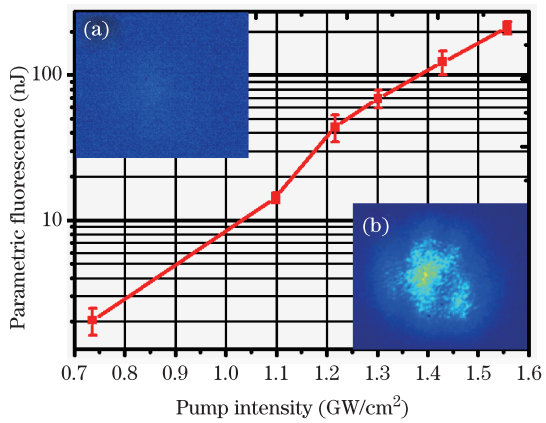

Fig. 3. Experimental results of parametric fluorescence versus different pump intensities. Insets (a) and (b) are images of parametric fluorescence corresponding to 0.74- and 1.56-GW/cm^2 pump intensities, respectively.

The optical gain of the IR image versus the pump intensities is measured as the laser beam intensity gradually increases, as shown by the blue solid curve in Fig. 2. More than six orders of magnitude (60 dB) gain is obtained when the pump intensity exceeds 1.25 GW/cm^2. To simulate this process, a numerical model is established by applying the three-wave coupling equations to the OPA[12], and the energy gain versus the pump intensity is numerically simulated and plotted in the red dashed curve with square dots. The output image without and with the OPA interaction is shown in insets (a) and (b) of Fig. 2, respectively. The circular distribution with three bars (corresponding to 2 lines/mm resolution) at the center is clearly observed after amplification. The numerical simulation and experimental results agree well at low pump intensity. However, the deviation between the experimental and simulation results becomes remarkable when the pump intensity is increased to more than 1.5 GW/cm^2. The simulation and experimental results under 1.56-GW/cm^2 pump intensity are 7.1×10^6 and 5.8×10^6, respectively. When these two values are 9.0×10^5 and 8.7×10^5, the pump intensity is 1.21 GW/cm^2.

The increasing deviation can be attributed to the rapid growth of the parametric fluorescence generated by optical parametric generation that starts from the quantum noise. The energy of the parametric fluorescence is measured with the nJ energy detector after the signal is blocked. The energy versus the pump intensity is shown in the red curve in Fig. 3. The curve indicates that even if the parametric fluorescence is efficiently suppressed with the SF (a 1.0-mm aperture; GCM-5702M, CDHC-optics), its energy still increases by two orders of magnitude from 2.1 to 212.3 nJ when the pump intensity increases from 0.74 to 1.56 GW/cm^2. Insets (a) and (b) of Fig. 3 show the corresponding spatial distribution of the parametric fluorescence. Given that the increase in the parametric fluorescence deteriorates the output image, a tradeoff between the parametric gain and the fluorescence intensity should be reached, and the pump power intensity is not further increased.

The transverse resolution is further investigated based on the resolution chart. The different parts on the resolution chart are illuminated one by one by a laser because of the limited field of view (FOV) of our imaging module. The amplified images are shown in Fig. 4, in which the images from the first to the fourth row correspond to 2, 4, 6, and 8 lines/mm resolutions, respectively. The images with 2 to 6 lines/mm resolutions are well recognized. Considering the limit of acceptance angle of BBO, the resolution limit is approximately 8 lines/mm, as shown in the bottom part of Fig. 4.

Detection sensitivity is the most critical issue in several applications. Therefore, the detection limit of OPA-assisted CCD is examined in our experiment. Considering that the 2 lines/mm region on the resolution chart is selected as the input image, the original image contains three bars in the FOV. Although the increasing pump intensity leads to a larger optical gain, it also leads to a larger parametric fluorescence. Accordingly, a pump intensity of 1.44 GW/cm^2 is selected through the experimental optimization. In the experiment, the original image is not detectable without OPA when the pulse energy is less than 1.9 pJ. The input signal is further reduced with the combination of ATT and NDFs. The amplified and frequency up-converted image with different input signals are plotted in Fig. 5. Although the SF is also introduced to suppress the parametric fluorescence, the amplified image is blurred by the background when the input signal becomes weaker. When the input signal is reduced to fJ scale, the output image becomes seriously blurry. In our experiment, the signal is reduced to 1.8 fJ per pulse with optical density of 10.9. This signal is more than three orders of magnitude weaker than the lowest detectable level of CCD at 1064 nm.

To further improve the detection sensitivity, the parametric fluorescence suppression should be the first priority. Approaches such as spatial filtering and non-collinear OPA could be used, especially in the fs region[13,14]. Meanwhile, for the signal laser with higher repetition rate, a lock-in amplifier could be used to improve the signal-to-noise ratio (SNR). For instance, when the laser repetition rate is 1000 Hz, a weak amplified signal submersed in the parametric fluorescence background can be recovered with a lock-in amplifier and a mechanical chopper modulating at 100 Hz. The amplified signal can be easily extracted from the background noise, which is not temporally modulated, by filtering the frequencies[15].

To enhance the transversal resolution, the imaging module and NLC could be optimized. Firstly, NLCs with

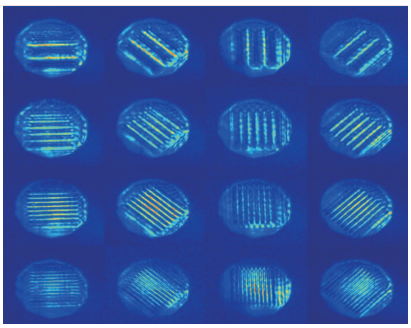

Fig. 4. Resolution chart of the amplified images. Images from the top to the bottom row correspond to the 2, 4, 6, and 8 lines/mm resolutions, respectively.

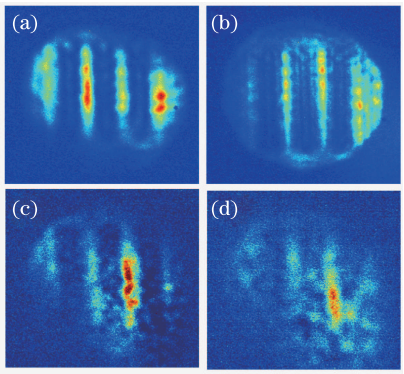

Fig. 5. Output up-converted images at 532 nm from CCD with 1.4-GW/cm^2 pump intensity under different seed infrared injections of (a) 1.5 pJ, (b) 90.4 fJ, (c) 11.7 fJ, and (d) 1.8 fJ.

larger acceptance angle are needed because the acceptance angle of the BBO is too small to obtain a higher transversal resolution. For instance, for the pump beam at a longer wavelength, such as 532 nm, LiB_3O_5 is a good candidate because of its larger acceptance angle. The advantage of frequency up-conversion can be optimized by converting the IR signal to the spectral region around 800 nm. This signal is more sensitive for the CCD camera by selecting an appropriate set of pump and signal wavelengths. Secondly, a proper imaging magnification can be selected when a Gaussian distribution of the pump beam is replaced with a flat-top distribution, and the uniformity of the output image can be improved. Moreover, a well designed image lens groups, instead of simple single lens, allow higher resolution.

In conclusion, using a BBO-based OPA in the ps region, we demonstrate an optical image amplifier with a 60-dB gain, which is two orders of magnitude higher than previously reported values. The lowest detectable image energy can be reduced to sub-10 fJ per pulse, indicating that the detection limit of an ordinary camera could be extended by OPA. The OPA-based image amplifier could provide an alternative approach for the electron multiplying CCD for sensitive imaging by effective suppression of the parametric fluorescence. Techniques for higher resolution and higher detection sensitivity are also proposed. In addition, the detectable wavelength can be significantly extended to IR or mid-IR region as long as the NLC permits.

This work was supported by the State Key Program for Basic Research of China (No. 2010CB630706) and the Knowledge Innovation Program of Chinese Academy of Sciences.

References

1. Y. Fainman, E. Klancnik, and S. H. Lee, Opt. Eng. **25,** 228 (1986).
2. J. A. Moon, R. Mahon, M. D. Duncan, and J. Reintjes, Opt. Lett. **19,** 1234 (1994).
3. S. Sternklar, S. Jackel, D. Chomsky, and A. Zigler, Opt. Lett. **15,** 616 (1990).
4. J. E. Midwinter, Appl. Phys. Lett. **12,** 68 (1968).
5. J. Watson, P. Georges, T. Lepine, B. Alonzi, and A. Brun, Opt. Lett. **20,** 231 (1995).
6. P. M. Vaughan and R. Trebino, Opt. Express **19,** 8920 (2011).
7. F. Devaux, E. Lantz, A. Lacourt, D. Gindre, H. Maillotte, P. A. Doreau, and T. Laurent, Nonlinear Opt. **11,** 25 (1995).
8. J. Yang, S. F. Du, J. Y. Zhang, D. Cao, D. F. Cui, Q. J. Peng, and Z. Y. Xu, Chin. Phys. Lett. **29,** 4213 (2012).
9. F. Devaux and E. Lantz, Eur. Phys. J. D **8,** 117 (2000).
10. F. Devaux and E. Lantz, Opt. Commun. **114,** 295 (1995).
11. F. Devaux and E. Lantz, J. Opt. Soc. Am. B **12,** 2245 (1995).
12. V. Smith, W. J. Alford, T. D. Raymond, and M. S. Bowers, J. Opt. Soc. Am. B **12,** 2253 (1995).
13. J. Zhang, A. P. Shreenath, M. Kimmel, E. Zeek, R. Trebino, and S. Link, Opt. Express **11,** 601 (2003).
14. J. Zhang, Q. Zhang, K. Qiu, D. Zhang, B. Feng, and J. Zhang, Opt. Commun. **291,** 329 (2013).
15. X. Han, Y. Weng, R. Wang, X. Chen, K. Luo, L. Wu, and J. Zhao, Appl. Phys. Lett. **92,** 151109 (2008).